INTERNATIONAL JOURNAL OF HYDROGEN ENERGY 48 (2023) 39944–39953

Available online at www.sciencedirect.com

ScienceDirect

journal homepage: www.elsevier.com/locate/he

Boosting borohydride hydrolysis for H_2 generation by MOF-templated void-engineered shaggy cobalt oxide: Abundant oxygen vacancy-mediated enhancement

Duong Dinh Tuan [a], *Huu Tap Van* [b,c], *Dang Thi Thai Ha* [a], *Jet-Chau Wen* [d], *Eilhann Kwon* [e], *Suresh Ghotekar* [f], *Bui Xuan Thanh* [g,l], *Jechan Lee* [h,**], *Yiu Fai Tsang* [i], *Kun-Yi Andrew Lin* [j,k,*]

[a] *International School, Thai Nguyen University, Thai Nguyen, 250000, Viet Nam*

[b] *Faculty of Natural Resources and Environment, TNU – University of Sciences, Tan Thinh ward, Thai Nguyen City, Viet Nam*

[c] *Center for Advanced Technology Development, Thai Nguyen University, Tan Thinh ward, Thai Nguyen City, Viet Nam*

[d] *National Yunlin University of Science and Technology, Douliu, Yunlin County, Taiwan*

[e] *Department of Earth Resources and Environmental Engineering, Hanyang University, SeongDong-Gu, Seoul, South Korea*

[f] *Centre for Herbal Pharmacology and Environmental Sustainability, Chettinad Hospital and Research Institute, Chettinad Academy of Research and Education, Kelambakkam 603103, Tamil Nadu, India*

[g] *Key Laboratory of Advanced Waste Treatment Technology & Faculty of Environment and Natural Resources, Ho Chi Minh City University of Technology (HCMUT), Ho Chi Minh City, Vietnam*

[h] *Department of Global Smart City & School of Civil, Architectural Engineering, and Landscape Architecture, Sungkyunkwan University, Suwon, 16419, Republic of Korea*

[i] *Department of Science and Environmental Studies, The Education University of Hong Kong, Tai Po, New Territories 999077, Hong Kong*

[j] *Department of Environmental Engineering & Innovation and Development Center of Sustainable Agriculture, National Chung Hsing University, Taichung, Taiwan*

[k] *Institute of Analytical and Environmental Sciences, National Tsing Hua University, Hsinchu, Taiwan*

[l] *Vietnam National University Ho Chi Minh City (VNU-HCM), Linh Trung ward, Ho Chi Minh City 700000, Vietnam*

* *Corresponding author*. Department of Environmental Engineering & Innovation and Development Center of Sustainable Agriculture, National Chung Hsing University, Taichung, Taiwan.

** *Corresponding author*.

E-mail addresses: jechanlee@skku.edu (J. Lee), linky@nchu.edu.tw (K.-Y.A. Lin).

https://doi.org/10.1016/j.ijhydene.2023.08.059

HIGHLIGHTS

- Void and shaggy-structured Co_3O_4 (VSCO) is created by a facile carving treatment.
- VSCO exhibits more superior textural properties than commercial Co_3O_4 NP (CCON).
- VSCO also possesses more abundant oxygen vacancies than CCON.
- VSCO enables a significantly low E_a of H_2 generation from $NaBH_4$ hydrolysis.
- VSCO remains highly effective for catalyzing $NaBH_4$ hydrolysis over 5 cycles.

GRAPHICAL ABSTRACT

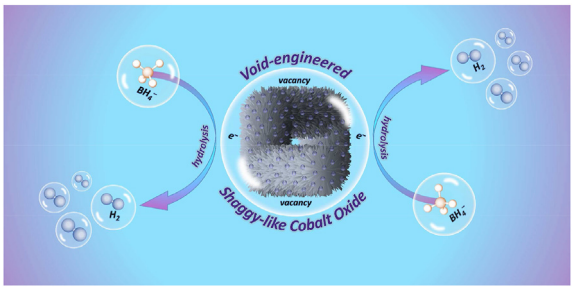

ARTICLE INFO

Article history:
Received 14 March 2023
Received in revised form
28 July 2023
Accepted 5 August 2023
Available online 01 September 2023

Keywords:
H_2
$NaBH_4$
Hydrolysis
Cobalt oxide
Oxygen vacancy

ABSTRACT

Designing an advantageous catalyst for enhancing the release of hydrogen (H_2) from $NaBH_4$ hydrolysis is still desirable. Herein, a void-engineered shaggy cobalt oxide (VSCO) is constructed via facile carving and calcination using the cuboid cobalt-based metal organic framework (Co-MOF) as a template. The as-prepared VSCO shows unique structural properties, such as large internal void, high specific surface area, and abundant oxygen vacancy, enabling VSCO to boost H_2 production from $NaBH_4$ hydrolysis. VSCO also exhibits an activation energy (E_a) of 28.9 kJ mol^{-1}, which is much lower than that of commercial Co_3O_4 NP (62.9 kJ mol^{-1}) and most of recent reported noble metals. VSCO also retains its outstanding catalytic activity over multiple cycles. This work sheds a light into the new approach of constructing metal oxide material with the void structure and abundant oxygen vacancies for catalyzing the hydrolysis of $NaBH_4$.

1. Introduction

The vast growth of industrialization and urbanization leads to the overconsumption of energy where fossil fuels account for over 80% the total demand [1,2]. As a result, the emissions released from burning of fossil fuels are ascribed as the significant cause for air pollution, ozone depletion, and global warming, which subsequently cause negative effects on human health. Thus, seeking potential green alternative energy sources to replace conventional fossil fuels is imperative. Amongst numerous alternative energies, hydrogen (H_2) is considered as the most promising candidate due to its abundance, environmental-friendliness, and non-carbon emission [3]. Nevertheless, the utilization of hydrogen for commecial purposes is restricted by the storage and transportation path, in which physical storage methods such as compression and liquefaction are commonly employed, resulting in high-cost and safety risks [4]. In contrast to physical storage, chemical hydrides (e.g., MgH_2, $LiAlH_4$, $NaBH_4$) appears to be potential hydrogen carriers for practical applications due to their advantages of safety concerns and high-purity generated H_2 at mild conditions [5–7]. Amid them, sodium borohydride ($NaBH_4$) has been gained increasing attention because of its exceptional theoretical H_2 storage capacity (10.8 wt%), low-toxicity, easy handling, stability in alkaline medium, and recycle capability [8,9].

Hydrolysis of $NaBH_4$ is believed to be the most effective technique for releasing high-purity H_2 in the presence of appropriate catalysts [10]. While noble metal catalysts (e.g., platinum (Pt) [11], palladium (Pd), ruthenium (Ru) [12,13]) exhibit outstanding activities of $NaBH_4$ hydrolysis for H_2 production, their applications are limited by their high costs and rare availability. Recently, non-noble transition metal catalyst (e.g., copper (Cu), nickel (Ni), cobalt (Co)) have been commonly employed for enhacing H_2 production from $NaBH_4$ hydrolysis, in particular, Co-based catalysts stands out as the most effective candidate [14–17]. However, the development of useful Co-based catalysts with superior structures and catalytic activities for catalyzing hydrolysis of $NaBH_4$ is still desired. Herein, we propose a novel intriguing Co-based catalyst using a cuboid Co-metal organic framework (Co-MOF) as a template.

Through a two-step modification of carving and calcination, Co-MOF could be transformed into a void-engineered shaggy cobalt oxide (denoted as VSCO). Characterizations are performed to reveal the special morphology with the void structure, high specific surface area, and abundant oxygen vacancy in VSCO, which then promote its catalytic activity to boost H_2 generation from $NaBH_4$ hydrolysis. Besides, the effects of other influential parameters are also studied to determine the optimal hydrolysis conditions. Then, the hydrolysis mechanism is also proposed based on the Michaelis-Menten mechanism [18]. More importantly, VSCO would be comprehensively compared with commercial cobalt oxide nanoparticle (CCON) for unraveling the structure-property relationship to probe into the advantage of the special morphology and surficial properties of VSCO.

2. Experimental

The synthesis procedure of VSCO is schematically illustrated in Fig. 1. In general, Co-MOF was first prepared by assembling cobalt ions and 2-MIM with the addition of CTAB as surfactant. Then, the as-prepared Co-MOF was immersed into gallic acid solution to afford a void-framework structure, followed by calcination in air [15,16,19,20]. The detailed preparation method and experimental procedures of H_2 generation from $NaBH_4$ hydrolysis can be found in the supporting information. The H_2 production rate (k) of hydrolysis reaction was calculated as the following equation [21]:

$$H_2 \text{ rate } (k) = V_{H_2} / (t \times m) \quad (1)$$

where m is the mass of catalyst (g), t represents reaction time (min) For further investigations, the effect of elevated temperatures on hydrolysis of $NaBH_4$ using both VSCO and CCON was performed. The activation energy (E_a) was then calculated via the Arrhenius equation as follows:

$$\ln k = \ln A - Ea / (R \times T) \quad (2)$$

where A, R, and T are pre-exponential constant, gas constant, and the reaction temperature (Kelvin), respectively.

3. Results and discussion

3.1. Physical and chemical properties of VSCO

The morphologies of the as-prepared materials were first visualized by electron microscopies including scanning electron microscopy (SEM) and transmission electron microscopy (TEM). As displayed in Fig. 2(A-B), the cuboid-structured Co-MOF was successfully constructed with external smooth surfaces and the size of Co-MOF ranges from 500 to 650 nm. After being modified by gallic acid, the smooth surfaces of Co-MOF turned into the shaggy morphology, but the cuboid appearance still remained (Fig. 2(C)). The TEM image in Fig. 2(D) further reveals that the solid structure of the pristine Co-MOF was transformed into the void structure, indicating the successful carving treatment. Moreover, as such a void-structured Co-MOF was further calcined, Fig. 2(E-F) shows that the resultant product still well-preserved the cuboid and void structure, whereas plenty of rounded particles could be also observed (Fig. 2(F)). The size of those particles was analyzed as shown in Fig. S1, indicating that they were nanoscale with the dominant size ranging from 7.8 to 12.1 nm. Its corresponding high-resolution TEM (HR-TEM) showed particular lattice d-spacing of 0.285 nm as well as 0.241 nm, that were indexed to the (220) and (311) crystal planes of Co_3O_4. This finding confirmed that these rounded nanoparticles (NPs) are Co_3O_4, and void-structured Co-MOF had been transformed into Co_3O_4, affording the void-engineered shaggy cobalt oxide (VSCO). The polycrystalline structure of VSCO was further determined based on the selected area electron diffraction (SAED) pattern in Fig. 2(H). Moreover, the chemistry of VSCO would be also examined as presented in Fig. S2, showing merely significant signals of Co as well as O were detected, assuring the composition of Co_3O_4 within VSCO.

To further verify the crystallinity, XRD analysis would be then performed. As displayed in Fig. 2(I), the as-prepared Co-MOF shows several notable diffraction peaks, which are well-indexed to the simulated Co-MOF [22–26], affirming the successful formation of Co-MOF. Next, the XRD profile of VSCO in Fig. 2(K) manifests totally different diffraction peaks. Specifically, numerous remarkable peaks at 19°, 31.3°, 36.9°, 38.6°,

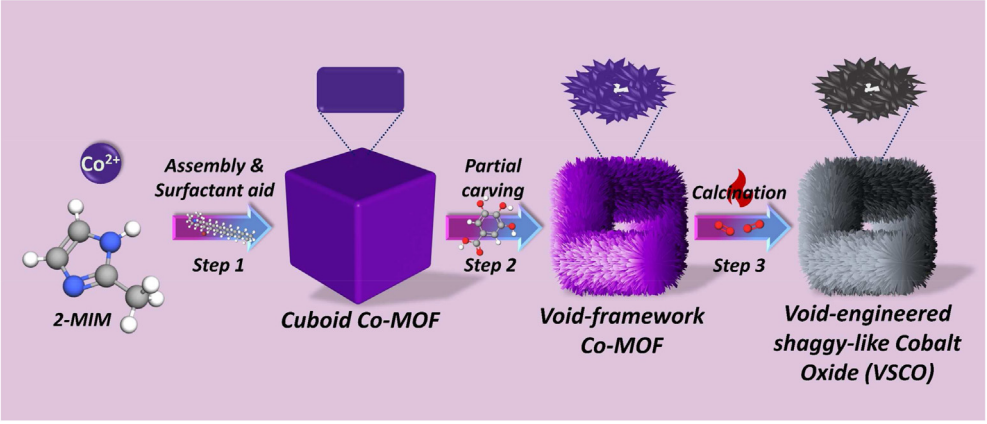

Fig. 1 – Schematic illustration for VSCO synthesis procedure.

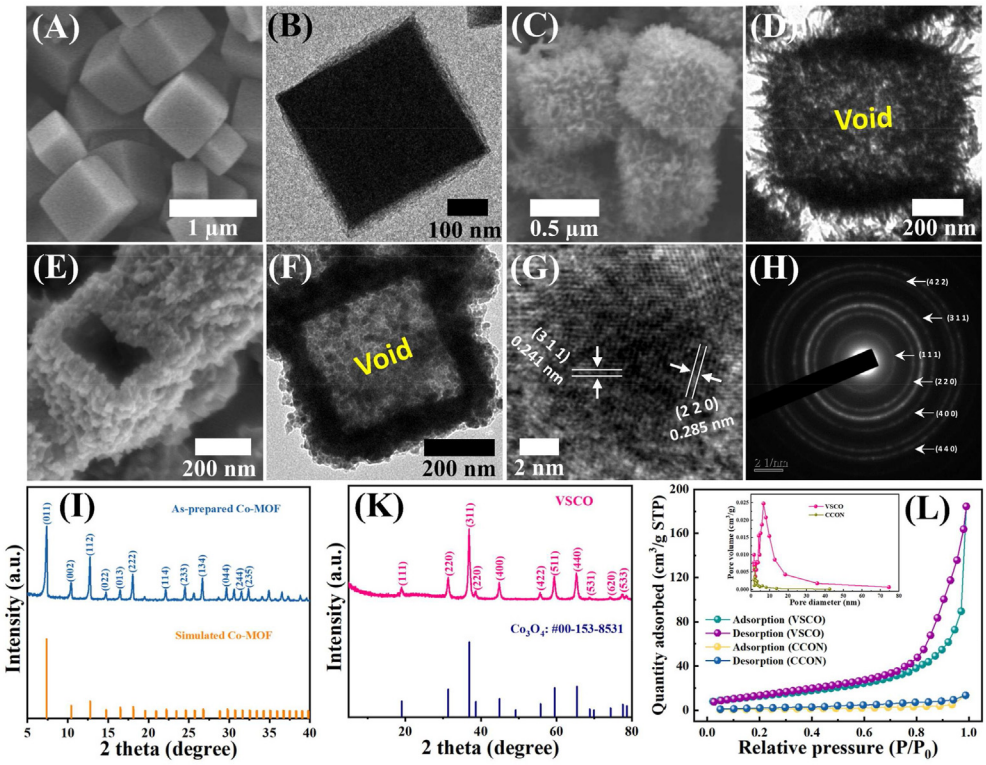

Fig. 2 – Microscopic analyses (A,B) of cuboid Co-MOF; (C–D) and void-structured Co-MOF; (E–F) SEM and TEM images of VSCO; (G–H) HR-TEM and SAD of VSCO; (I–K) XRD profiles of Co-MOF and VSCO; (L) N_2 adsorption-desorption isotherms of VSCO and CCON (the inset displays pore size distribution).

44.8°, 55.7°, 59.4°, 65.2°, 74.12° and 77.5° could be ascribed to the crystal planes of (111), (220), (311), (220), (400), (422), (511), (440), (620), and (533) of Co_3O_4 (JCDPS #00-153-8531), that are in line with the SAED analysis in Fig. 2(H), further assuring the transformation of Co-MOF into VSCO. Besides, the specific surface areas (SSA) and pore volume of VSCO and CCON were then verified by N_2 adsorption-desorption isotherms. It can be noticed from Fig. 2(L) that VSCO presents the type IV isotherm with an obvious hysteresis loop, suggesting the presence of mesopores. The inset in Fig. 2(L) presents the pore size distribution, further ascertaining that VSCO consisted of mesopores, and the SSA of VSCO was determined as 48.1 m^2/g with a 0.3 cc/g pore volume (Table S1). On the other hand, as CCON was also employed for catalyzing $NaBH_4$ hydrolysis, its textural properties were also characterized. As displayed in Fig. 2(L), CCON exhibited a very low N_2 adsorption amount, then its SSA was measured as merely 2.6 m^2/g with a pore volume of 0.002 cc/g. The low SSA and pore volume of Co_3O_4 NP could be ascribed to the aggregation of these NPs as displayed in Fig. S3.

In addition, Raman spectroscopies of VSCO and CCON were further characterized. Fig. 3(A) displays the wide-range Raman spectra, showing that both materials comprise of five typical Raman active vibration modes of A_{1g}, E_g, and $3F_{2g}$ of Co_3O_4 [27], proving that VSCO possesses high crystallinity of Co_3O_4 after calcination process. Nevertheless, in the specific regions of F_{2g} and A_{1g} in Fig. 2(B) and (C), those peaks in VSCO were shifted to lower frequencies compared with those of CCON. In particular, the peak of F_{2g} in VSCO shifted to 190 cm^{-1} while the peak of A_{1g} switched to 678 cm^{-1}. Since A_{1g} and F_{2g} could be ascribed to the coordination of Co^{2+} and Co^{3+} in the tetrahedron (CoO_4) and octahedron (CoO_6) sites of Co_3O_4, respectively, these shifts suggest that VSCO contains defective sites or oxygen vacancies [28]. Moreover, XPS analysis was carried out to study the chemical surface and valence states of VSCO and CCON. As presented in Fig. 3(D), both materials exhibited similar patterns in the wide-range spectra whereas Co and O signals were detected in VSCO, which is well-correlated with EDX analysis. Besides, Fig. 3(E) shows the high-resolution XPS spectra of Co 2p of VSCO and CCON in which Co 2p spectra could be split up into 2p3/2 (779.8 eV) and 2p1/2 (794.8 eV) with satellite peaks [29]. Then, these peaks can be further deconvoluted into multiple underlying peaks. Specifically, those underlying peaks centered at 779.4 as well as 794.6 eV were assigned to Co^{3+} whereas those positioned at 781.4 as well as 797 eV were ascribed to Co^{2+}. Furthermore, the high-resolution spectra of O 1s of VSCO and CCON were displayed in Fig. 3(F). It can be observed that O 1s spectra in CCON can be deconvoluted into two fitting peaks at 529.5 eV and 531.3 eV attributed to the lattice O (O_{latt}) as well as adsorbed O (O_{ads}). In contrast to CCON, O 1s spectra of VSCO can be divided into three fitting peaks positioned at 529.6 eV, 531 eV, and 533 eV attributing to O_{latt}, oxygen vacancy (O_{vac}), and O_{ads} [30]. This further affirms the existence of oxygen vacancy in the structure of VSCO, which is consistent with Raman analysis.

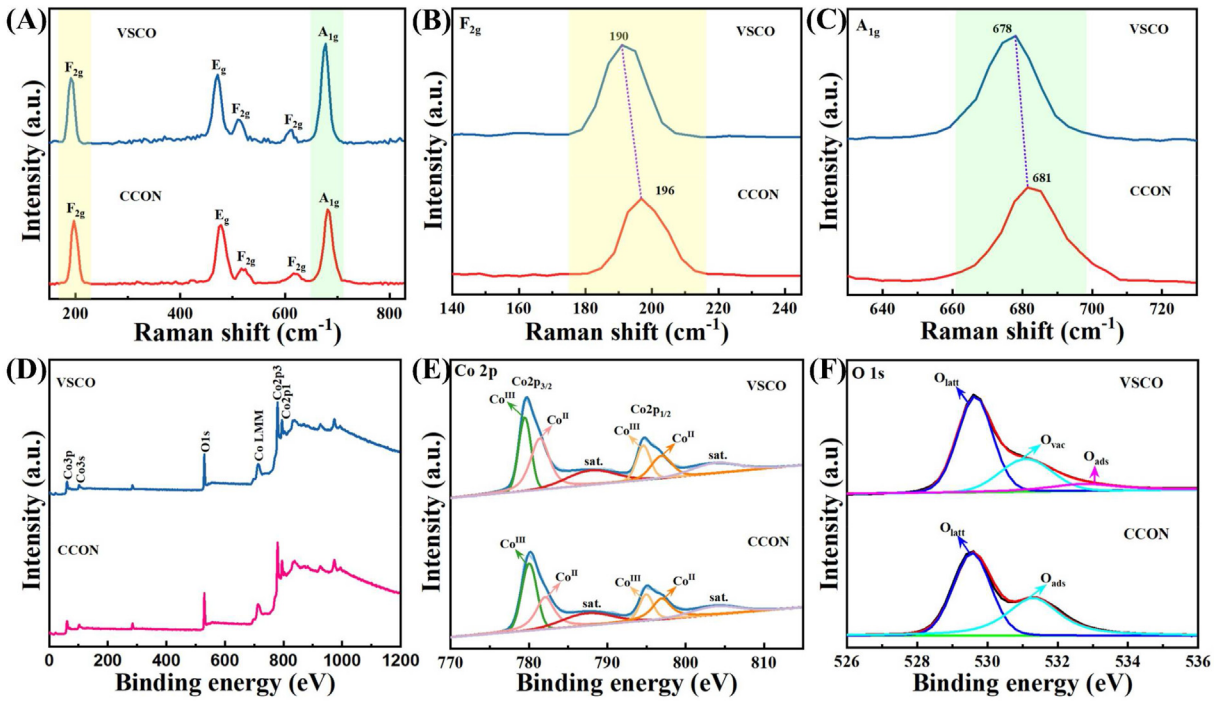

Fig. 3 – (A–C) Raman spectra of VSCO and CCON: (A) wide-range spectra, (B) and (C) spectra at specific F_{2g} and A_{1g} regions; (D–E) XPS profiles of VSCO and CCON: (D) wide-scanning spectra, (E–F) high-resolution spectra of Co 2p and O 1s.

3.2. *Catalytic hydrolysis of $NaBH_4$ using VSCO*

3.2.1. *General comparison*

Prior to assessing the catalytic performance of VSCO for hydrolysis of $NaBH_4$ to produce H_2, it would be imperative to evaluate the self-hydrolysis of $NaBH_4$ for H_2 production. In Fig. 4(A), deficient H_2 volume was generated in case of $NaBH_4$ only with a low *k* value of 84.8 mL/min/g (Fig. 4(B)). This indicates that without the addition of catalysts, H_2 production from $NaBH_4$ self-hydrolysis was inefficient. Besides, Co-MOF, the precursor of VSCO, was also utilized to catalyze the hydrolysis of $NaBH_4$. Nonetheless, H_2 production was still very limited as its corresponding *k* value was only 112.6 mL/min/g. In the case of CCON, it can be noticed that H_2 production efficiency from $NaBH_4$ hydrolysis was slightly improved since 129 mL of H_2 could be generated in 14 min with the corresponding *k* increased to 461.2 mL/min/g, verifying the capability of CCON for hydrolyzing $NaBH_4$. In addition to CCON, VSCO could dramatically enhance H_2 production capability as 440 mL of H_2 (equilibrium level) (98% of the theoretical volume) could be produced and the corresponding *k* value reached to 1571.4 mL/min/g, which is 3.4 times the k of CCON, possibly attributed to the difference of the textural properties and abundant oxygen vacancy between VSCO and CCON as discussed in section 3.1. This result manifests the outstanding activity of VSCO for boosting H_2 production efficiency from the hydrolysis of $NaBH_4$. On the other hand, to unveil the practical application of VSCO for the hydrolysis of $NaBH_4$, we conducted an additional experiment using VSCO without predisperson. As shown in Fig. S4, the H_2 production

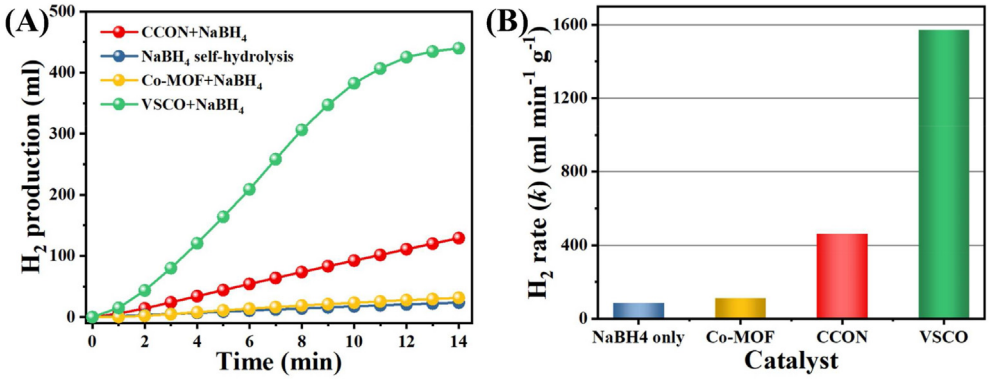

Fig. 4 – (A) H_2 production from $NaBH_4$ hydrolysis using different catalytic systems, and (B) the corresponding calculated H_2 production rate (*k*) by these systems. Conditions: catalyst = 400 mg L^{-1}, $NaBH_4$ = 125 mM, T = 30 °C.

efficiencies in the case of with/without pre-dispersion were comparable, suggesting that VSCO could exhibit its outstanding performance without pre-dispersion step. This confirms the promising practical application of VSCO for H_2 production from $NaBH_4$ hydrolysis.

3.2.2. *Effect of temperatures*

To further elucidate the superior catalytic activity of VSCO for catalyzing $NaBH_4$ hydrolysis, the effect of temperature on H_2 production using VSCO was then performed. In Fig. 5, H_2 could reach to the equilibrium level within shorter reaction times by VSCO as the temperature increased from 30 °C (14 min) to 40 °C (10 min), 50 °C (7 min), and 60 °C (5 min). The corresponding k values at temperatures (Fig. 5(B)) were 1571.4 mL/min/g at 30 °C, 2200 mL/min/g at 40 °C, 3142.9 mL/min/g at 50 °C, and 4400 mL/min/g at 60 °C, respectively. On the other hand, in the case of CCON, H_2 production efficiencies were also improved (Fig. 5(D)) as H_2 could also reach to the equilibrium level within shorter reaction times at higher temperatures (i.e., 50 °C (12 min), 60 °C (8 min)) with higher k values (Fig. 5(E)).

Next, the relationships between temperatures and k values of VSCO and CCON were correlated and illustrated in Fig. 5(C) and (F). It can be noticed that both the data of VSCO and CCON would be well-fit by linear regression of $R^2 > 0.99$, and E_a values were subsequently determined as 28.9 kJ mol^{-1} and 62.9 kJ mol^{-1} for VSCO and CCON, respectively. This further validates the advantageous performance of VSCO over CCON to catalyze the hydrolysis of $NaBH_4$ for producing H_2. Moreover, E_a values of VSCO and other recent reported catalysts were also summarized in Table S3, signifying that VSCO exhibited a lower E_a value than most recent catalysts, even noble-metal ones. This further proves that VSCO would be a useful as well as highly efficient for H_2 generation.

3.2.3. *Effects of VSCO dosages, $NaBH_4$ dosages, NaOH concentrations, and recyclability test*

In addition to temperatures, other influential parameters on H_2 production from $NaBH_4$ hydrolysis were then examined in Fig. 6. The effect of different VSCO dosages was first performed. From Fig. 6(A), H_2 production efficiencies were obviously enhanced when VSCO dosage increased. Specifically, as discussed previously, very low H_2 volume could be generated in the absence of VSCO. However, once a small amount of VSCO (i.e., 200 mg L^{-1}) was introduced, nearly 400 mL of H_2 could be achieved in 14 min. When the dosage of VSCO increased, H_2 could reach to the equilibrium level in shorter times at higher dosages of VSCO. The higher corresponding k values were also measured in Fig. S5(A), indicating the positive influence of higher VSCO dosages to $NaBH_4$ hydrolysis.

Besides, the effect of various $NaBH_4$ amounts was also investigated. As displayed in Fig. 6(B), higher H_2 production volume could be obtained with the increase in $NaBH_4$ amounts from 100 mM to 250 mM. More importantly, the initial hydrolysis stages of these H_2 production curves were overlapped, suggesting that k values at the beginning hydrolysis procedure were similar. While excessive $NaBH_4$ concentrations may produce more by-products (e.g., sodium metaborate ($NaBO_2$)) that increases the solution viscosity, blocking active surface sites and diminishing H_2 production efficiency [16], the result above indicates that VSCO could retain its outstanding catalytic activity, even at high $NaBH_4$ concentrations.

Moreover, since NaOH is considered as a stabilizing agent to avoid the self-hydrolysis of $NaBH_4$ [31], the influence of addition of NaOH to $NaBH_4$ hydrolysis for H_2 production was further investigated. H_2 production might be facilitated by the slight addition of NaOH using cobalt-based catalysts [32,33]; in Fig. 6(C), the addition of NaOH certainly influenced H_2

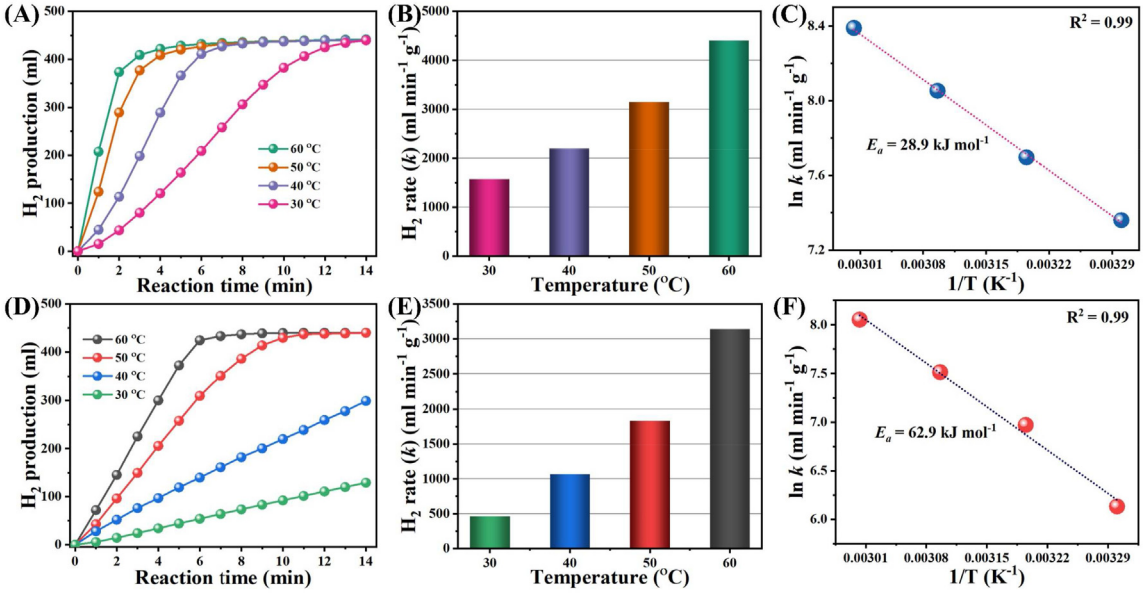

Fig. 5 – A comparison between VSCO and CCON: (A) and (D) H_2 production at various temperatures, (B) and (E) the corresponding calculated H_2 production rates (k), (C) and (F) the corresponding calculated activation energies (E_a) (kJ mol^{-1}). Conditions: catalyst = 400 mg L^{-1}, $NaBH_4$ = 125 mM.

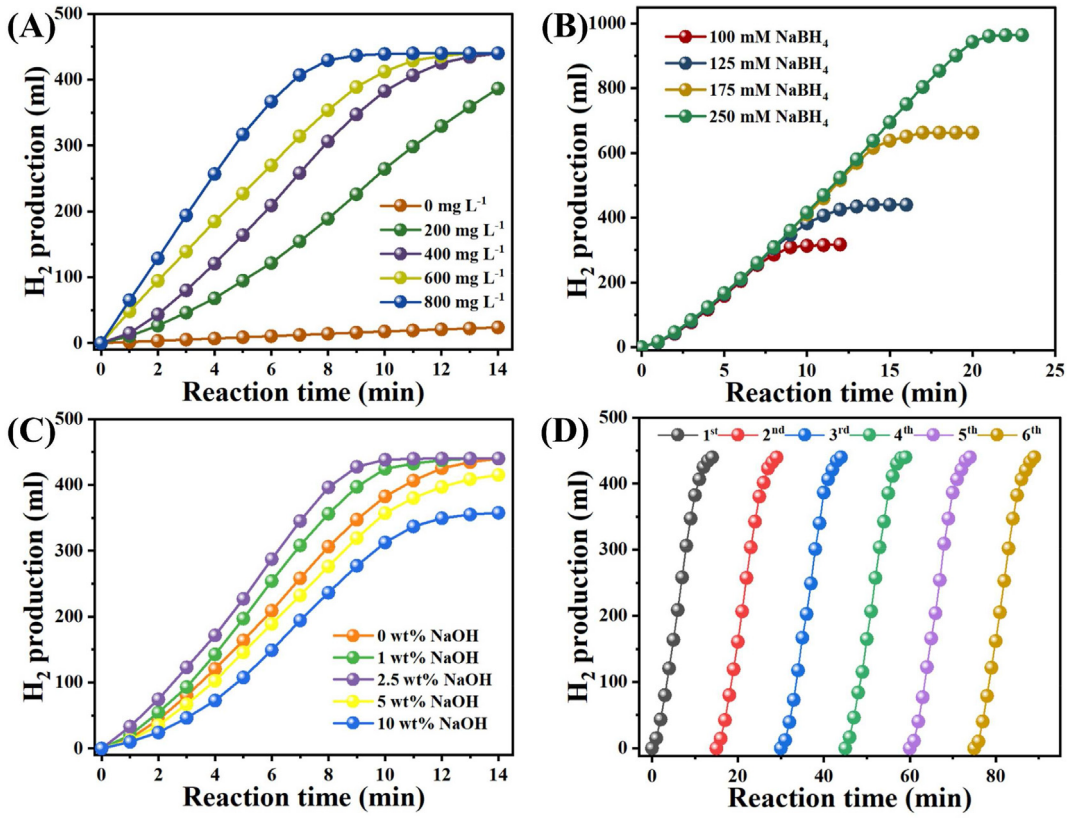

Fig. 6 – (A) effect of different VSCO dosages, (B) effect of various $NaBH_4$ amounts, and (C) effect of different NaOH concentrations on H_2 production; (D) recyclability test of VSCO for continuous catalyzing hydrolysis of $NaBH_4$. Conditions: VSCO = 400 mg L^{-1}, $NaBH_4$ = 125 mM, T = 30 °C.

production efficiency. Particularly, at 1 wt% of NaOH, H_2 could be produced faster as its *k* value increased to 1833.3 mL/min/g, which was further raised to 2200 mL/min/g at 2.5 wt% of NaOH (Fig. S5(B)), demonstrating that low NaOH concentrations would be favorable for facilitating H_2 production. Nonetheless, when NaOH concentration increased to 5 wt% and 10 wt%, slower H_2 production could be observed with the corresponding *k* values were determined as 1482.8 mL/min/g and 1277 mL/min/g, respectively. This result reveals that excessive NaOH amounts might cause negative influence on the hydrolysis of $NaBH_4$. These phenomena were possibly because: (1) OH^- anions dissociated from NaOH at a low concentration might enhance the dispersion of catalyst, then enhancing H_2 production rates [16,34]; (2) OH^- ions on the surface can stimulate the cleavage of O–H bond in H_2O [35]; (3) the presence of OH^- could be further ascribed to its coordination with the surface of the catalyst by increasing the electron density and subsequently allow the oxidative addition of the O–H bond [36]. In contrast, high NaOH concentrations might intensify the alkalinity and subsequently increase the solution viscosity, inhibiting the catalytic hydrolysis of $NaBH_4$ [37]. In view of these results, the NaOH concentration of 2.5 wt% would be the optimal NaOH concentration in this study.

Besides, as VSCO exhibited outstanding catalytic capability for producing H_2 from $NaBH_4$ hydrolysis, it would be imperative to evaluate the reusability of VSCO. Fig. 6(D) reveals that comparable H_2 yields were still achieved over the multiple cycles using the used VSCO, validating that VSCO could well-retain its catalytic activity. Moreover, the morphology of used VSCO was also characterized as indicated in Figs. S6(A) and (B), signifying that void and shaggy structure of VSCO was still preserved. Additionally, the chemical states of used VSCO were then examined. Fig. S7 shows the wide-scanning spectra before and after hydrolysis reaction, indicating that Co and O signals were still retained. High-resolution Co 2p spectra of VSCO in Fig. 7(A) verifies that the content of Co^{2+} was slightly increased whereas that of Co^{3+} was moderately decreased, suggesting that partial Co^{3+} was reduced during the hydrolysis reaction. On the other hand, Fig. 7(B) also displays that the ratio of oxygen species was also slightly changed, in which both O_{latt} and O_{vac} contents were reduced while O_{ads} was slightly increased after hydrolysis reaction. Then, the hydrolysis reaction using VSCO-catalyzed $NaBH_4$ was schemed as presented in Fig. 7(C).

To further distinguish behaviors of CCON and VSCO, the active sites of the catalysts were then determined by measuring their electrochemical surface areas (ECSA). Specifically, the double layer capacitances (C_{DL}) of CCON and VSCO were firstly obtained by collecting scan rate-dependent CV curves of CCON and VSCO in the non-Faradaic region from

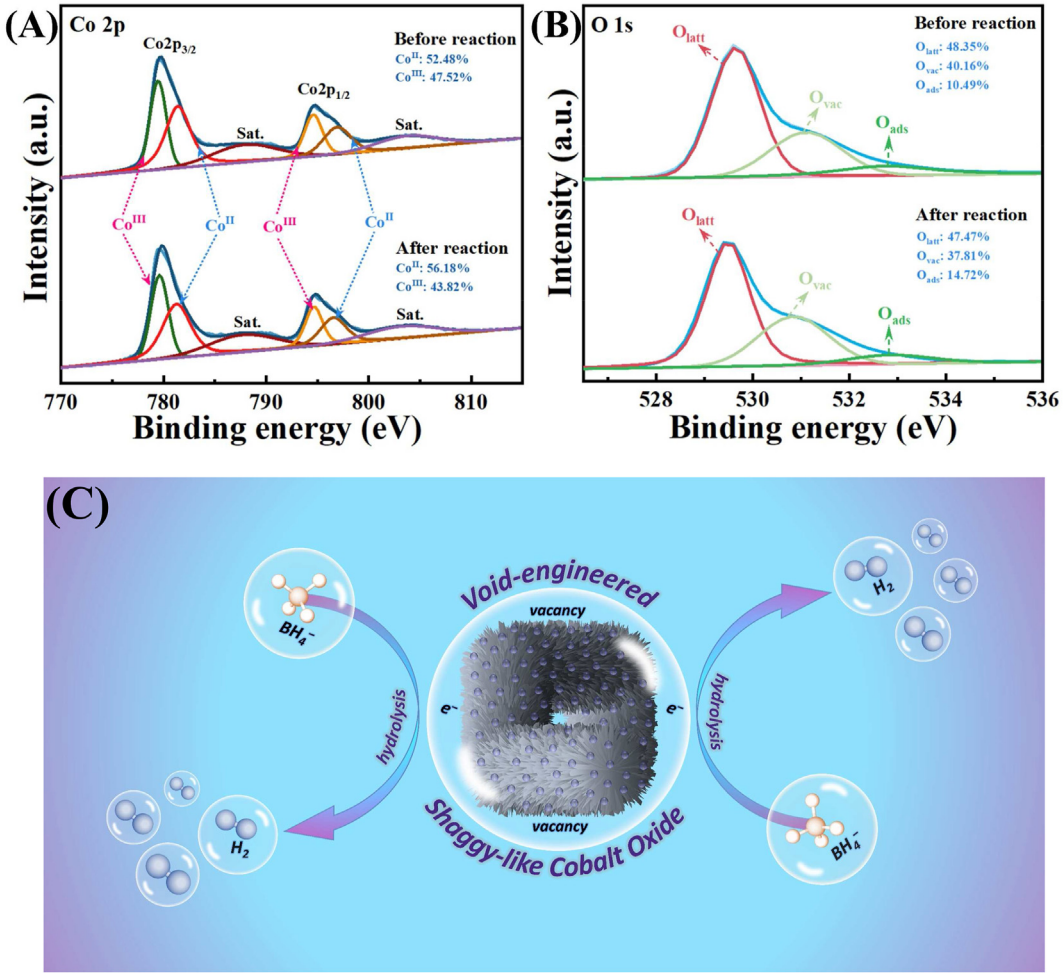

Fig. 7 – High-resolution XPS spectra of (A) Co 2p and (B) O 1s of VSCO before and after catalyzing hydrolysis of $NaBH_4$; (C) reaction scheme for releasing H_2 using VSCO-catalyzed hydrolysis of $NaBH_4$.

0.35 to 0.45 V in Figs. S8(a and b). The C_{DL} value was computed from $C_{DL} = J_m/\upsilon$, where J_m represents current density obtained from averaged values between the anodic and cathodic current densities according to the following Eq. (3) [38]

$$J_m = (|J_a| + |J_c|)/2 \quad (3)$$

whereas υ denotes the scan rate. By regressing the current density with the scan rate, the slope of the fitted plot (C_{DL}) was expressed in Fig. S8(c), in which the much higher C_{DL} value of 6.9 mF/cm^2 was obtained by VSCO whereas that of CCON was only 0.2 mF/cm^2. Correspondingly, the ECSA of VSCO was then calculated using Eq. (4) as 12.1 cm^2, while that of CCON was merely 0.4 cm^2, confirming that VSCO had more active site areas than CCON.

$$ECSA = S.C_{DL}/C_s \quad (4)$$

where S is the working electrode area, C_s is the specific capacitance obtained from an ideal electrode. According to these results of electrochemical analysis, VSCO certainly exhibited the much-enhanced electron transfer process and active sites.

3.2.4. *Catalytic hydrolysis mechanism*

The mechanism for H_2 production from the hydrolysis of $NaBH_4$ using VSCO was proposed as demonstrated in Fig. 8. According to the Michaelis-Menten mechanism, the hydrolysis of $NaBH_4$ undergoes three main steps [18]. First, the neutral form of $NaBH_4$ would approach and be adsorbed onto the VSCO surface, where BH_4^-, released from the dissociation of $NaBH_4$, would be subsequently fragmented into BH_3^- ion and H atom during this dissociative adsorption. Then, the resulting negatively-charged BH_3^- ion would be transformed to H via the mediation by oxygen vacancies [13,39]. Subsequently, the adsorbed H atom would react with free H_2O to product an intermediate $BH_3(OH)^-$ and release H_2. The reaction would then proceed via the similar route until $B(OH)_4$ and $4H_2$ are

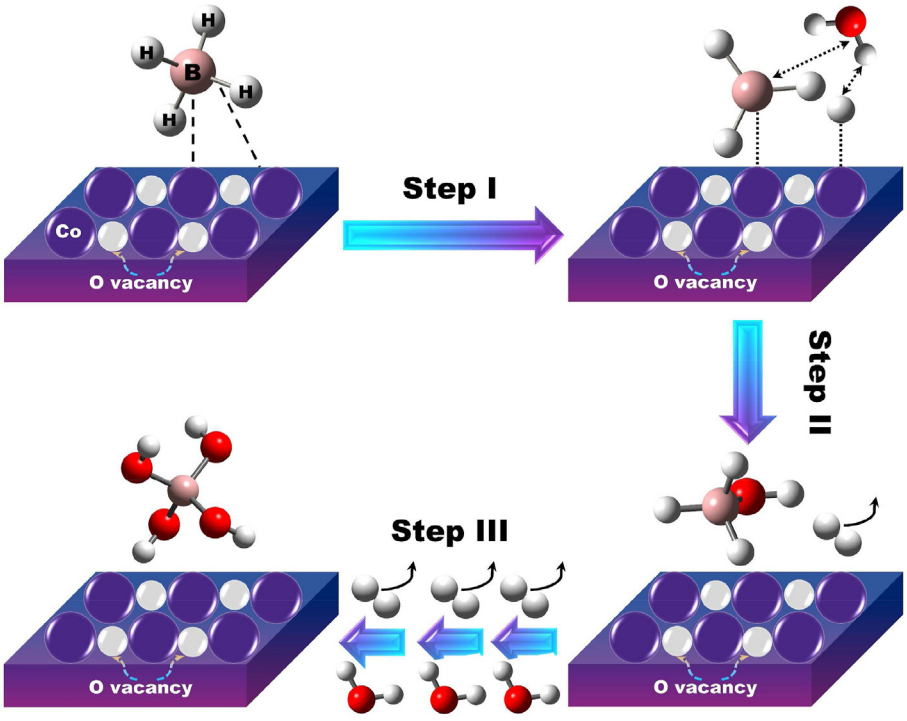

Fig. 8 – Proposed mechanism for releasing H_2 from the hydrolysis of $NaBH_4$ using VSCO.

produced [40]. Since VSCO possessed the higher degree of oxygen vacancies, VSCO would facilitate the process of converting BH_3^- to H, thereby enhancing H_2 generation.

4. Conclusion

In summary, we have successfully prepared the void-engineered shaggy cobalt oxide (VSCO) by using the cuboid Co-MOF as a template for catalyzing $NaBH_4$ hydrolysis to release H_2. The as-prepared VSCO exhibited intriguing textural properties as well as abundant oxygen vacancies in comparison with commercial Co_3O_4 NP (CCON). These distinct characteristics contributed to the different catalytic activities of VSCO and CCON for generating H_2. Specifically, VSCO exhibited a H_2 production rate of 1571.4 mL/min/g as well as E_a of 28.9 kJ mol^{-1} which was much lower than that of CCON (62.9 kJ mol^{-1}) and most recent reported catalysts, even noble metal catalysts in literature. VSCO could also retain its outstanding catalytic activity as well as intriguing structures over multiple cycles. This work also sheds a light into the new approach of constructing metal oxide materials with unique void-structure and abundant oxygen vacancy, which would be highly effective for H_2 production from hydrolyzing $NaBH_4$.

Declaration of competing interest

The authors declare that they have no known competing financial interests or personal relationships that could have appeared to influence the work reported in this paper.

Appendix A. Supplementary data

Supplementary data to this article can be found online at https://doi.org/10.1016/j.ijhydene.2023.08.059.

REFERENCES

[1] Xia Y, et al. Effects of various metal doping on the structure and catalytic activity of CoB catalyst in hydrogen production from NaBH4 hydrolysis. Fuel 2023;331:125733.
[2] Kıpçak İ, Kalpazan E. Preparation of CoB catalysts supported on raw and Na-exchanged bentonite clays and their application in hydrogen generation from the hydrolysis of NaBH4. Int J Hydrogen Energy 2020;45(50):26434–44.
[3] Shi L, et al. Carbon nanotubes-promoted Co–B catalysts for rapid hydrogen generation via NaBH4 hydrolysis. Int J Hydrogen Energy 2019;44(36):19868–77.
[4] Zhou S, et al. Structure-regulated Ru particles decorated P-vacancy-rich CoP as a highly active and durable catalyst for NaBH4 hydrolysis. J Colloid Interface Sci 2021;591:221–8.
[5] Kao H-Y, et al. Kinetics of hydrogen generation on NaBH4 powders using cobalt catalysts. J Taiwan Inst Chem Eng 2018;87:123–30.
[6] Ding Z, Zhao X, Shaw LL. Reaction between LiBH4 and MgH2 induced by high-energy ball milling. J Power Sources 2015;293:236–45.
[7] Wang YP, et al. Ultrafine amorphous Co–Fe–B catalysts for the hydrolysis of NaBH4 solution to generate hydrogen for PEMFC. Fuel Cell 2010;10(1):132–8.
[8] Peña-Alonso R, et al. A picoscale catalyst for hydrogen generation from NaBH4 for fuel cells. J Power Sources 2007;165(1):315–23.

[9] Ding C, et al. The coralline cobalt oxides compound of multiple valence states deriving from flower-like layered double hydroxide for efficient hydrogen generation from hydrolysis of NaBH4. Int J Hydrogen Energy 2021;46(2):2390–404.
[10] Abdelhamid HN. A review on hydrogen generation from the hydrolysis of sodium borohydride. Int J Hydrogen Energy 2021;46(1):726–65.
[11] Crisafulli C, et al. Hydrogen production through NaBH4 hydrolysis over supported Ru catalysts: an insight on the effect of the support and the ruthenium precursor. Int J Hydrogen Energy 2011;36(6):3817–26.
[12] Tuan DD, Lin K-YA. Ruthenium supported on ZIF-67 as an enhanced catalyst for hydrogen generation from hydrolysis of sodium borohydride. Chem Eng J 2018;351:48–55.
[13] Shi L, et al. Oxygen-vacancy-rich Ru-clusters decorated Co/Ce oxides modifying ZIF-67 nanocubes as a high-efficient catalyst for NaBH4 hydrolysis. Int J Hydrogen Energy 2022;47(89):37840–9.
[14] Demirci UB, Miele P. Cobalt-based catalysts for the hydrolysis of NaBH4 and NH3BH3. Phys Chem Chem Phys 2014;16(15):6872–85.
[15] Tuan DD, et al. Cobalt-based coordination polymer-derived hexagonal porous cobalt oxide nanoplate as an enhanced catalyst for hydrogen generation from hydrolysis of borohydride. Int J Hydrogen Energy 2020;45(56):31952–62.
[16] Tuan DD, Lin K-YA. ZIF-67-derived Co3O4 rhombic dodecahedron as an efficient non-noble-metal catalyst for hydrogen generation from borohydride hydrolysis. J Taiwan Inst Chem Eng 2018;91:274–80.
[17] Lin K-YA, Chang H-A. Efficient hydrogen production from NaBH4 hydrolysis catalyzed by a magnetic cobalt/carbon composite derived from a zeolitic imidazolate framework. Chem Eng J 2016;296:243–51.
[18] Demirci UB, Miele P. Reaction mechanisms of the hydrolysis of sodium borohydride: a discussion focusing on cobalt-based catalysts. Compt Rendus Chem 2014;17(7):707–16.
[19] Huang Y, et al. Co3O4 hollow nanoparticles embedded in mesoporous walls of carbon nanoboxes for efficient lithium storage. Angew Chem Int Ed 2020;59(45):19914–8.
[20] Lai H-K, et al. Coordination polymer-derived cobalt nanoparticle-embedded carbon nanocomposite as a magnetic multi-functional catalyst for energy generation and biomass conversion. Chem Eng J 2018;332:717–26.
[21] Wang C, et al. Electronic transfer enhanced coral-like CoxP loaded Ru nanoclusters as efficient catalyst for hydrogen generation via NaBH4 hydrolysis. Int J Hydrogen Energy 2022;48(4):1440–9.
[22] Lin K-YA, Chang H-A. Efficient adsorptive removal of humic acid from water using zeolitic imidazole framework-8 (ZIF-8). Water Air Soil Pollut 2015;226:10.
[23] Lin K-YA, Chang H-A. Ultra-high adsorption capacity of zeolitic imidazole framework-67 (ZIF-67) for removal of malachite green from water. Chemosphere 2015;139:624–31.
[24] Lin K-YA, Chang H-A. Efficient adsorptive removal of humic acid from water using zeolitic imidazole framework-8 (ZIF-8). Water, Air, Soil Pollut 2015;226:10.
[25] Lin K-YA, Chang H-A. Zeolitic Imidazole Framework-67 (ZIF-67) as a heterogeneous catalyst to activate peroxymonosulfate for degradation of Rhodamine B in water. J Taiwan Inst Chem Eng 2015;53:40–5.
[26] Lin K-YA, Chen S-Y. Catalytic reduction of bromate using ZIF-derived nanoscale cobalt/carbon cages in the presence of sodium borohydride. ACS Sustainable Chem Eng 2015;3(12):3096–103.
[27] Zhang Z, et al. Template free N-doped 3D porous carbon@Co3O4: towards highly efficient catalysis for peroxymonosulfate degradation of antibiotics. Opt Mater 2021;111:110538.
[28] Wang Z, et al. Surface oxygen vacancies on Co3O4 mediated catalytic formaldehyde oxidation at room temperature. Catal Sci Technol 2016;6(11):3845–53.
[29] Wang Q, et al. Two-dimensional ultrathin perforated Co3O4 nanosheets enhanced PMS-Activated selective oxidation of organic micropollutants in environmental remediation. Chem Eng J 2022;427:131953.
[30] Li P, et al. Defect-engineered Co3O4 with porous multishelled hollow architecture enables boosted advanced oxidation processes. Appl Catal B Environ 2021;298:120596.
[31] İzgi MS, et al. CeO2 supported multimetallic nano materials as an efficient catalyst for hydrogen generation from the hydrolysis of NaBH4. Int J Hydrogen Energy 2020;45(60):34857–66.
[32] Li Q, Kim H. Hydrogen production from NaBH4 hydrolysis via Co-ZIF-9 catalyst. Fuel Process Technol 2012;100:43–8.
[33] Ye W, et al. Hydrogen generation utilizing alkaline sodium borohydride solution and supported cobalt catalyst. J Power Sources 2007;164(2):544–8.
[34] Zhu J, et al. Fast hydrogen generation from NaBH4 hydrolysis catalyzed by carbon aerogels supported cobalt nanoparticles. Int J Hydrogen Energy 2013;38(25):10864–70.
[35] Fang S, et al. Modified CNTs interfacial anchoring and particle-controlled synthesis of amorphous cobalt-nickel-boron alloy bifunctional materials for NaBH4 hydrolysis and supercapacitor energy storage. J Alloys Compd 2023;936:167990.
[36] Luo C, et al. Highly efficient and selective Co@ZIF-8 nanocatalyst for hydrogen release from sodium borohydride hydrolysis. ChemCatChem 2019;11(6):1643–9.
[37] Prasad D, et al. Highly efficient hydrogen production by hydrolysis of NaBH4 using eminently competent recyclable Fe2O3 decorated oxidized MWCNTs robust catalyst. Appl Surf Sci 2019;489:538–51.
[38] Xu Z, et al. Understanding spatial effects of tetrahedral and octahedral cobalt cations on peroxymonosulfate activation for efficient pollution degradation. Appl Catal B Environ 2021;291:120072.
[39] Guo J, et al. Hierarchically structured rugae-like RuP3–CoP arrays as robust catalysts synergistically promoting hydrogen generation. J Mater Chem A 2019;7(15):8865–72.
[40] Guella G, et al. New insights on the mechanism of palladium-catalyzed hydrolysis of sodium borohydride from 11B NMR measurements. J Phys Chem B 2006;110(34):17024–33.